

Nanoscale Phase Separation Due to Doping and Electronic Degeneracies in Iron Pnictides

Vladimir Gnezdilov^{1,2,*}, Alexander Glamazda¹, Peter Lemmens², Kazutaka Kudo^{3,4} and Minoru Nohara⁵

¹B Verkin Institute for Low Temperature Physics and Engineering of the National Academy of Sciences of Ukraine, Kharkiv 61103, Ukraine

²Institute for Condensed Matter Physics, TU-Braunschweig, 38106 Braunschweig, Germany

³Department of Physics, Graduate School of Science, Osaka University, Toyonaka, Osaka 560-0043, Japan

⁴Institute for Open and Transdisciplinary Research Initiatives, Osaka University, Suita 565-0871, Japan

⁵Department of Quantum Matter, AdSE, Hiroshima University, Higashi-Hiroshima 739-8530, Japan

***Corresponding Author:** Vladimir Gnezdilov, B Verkin Institute for Low Temperature Physics and Engineering of the National Academy of Sciences of Ukraine, Kharkiv 61103, Ukraine, Tel.: +(38)-057 343 14 00, E-mail: gnezdilov@ilt.kharkov.ua

Citation: Vladimir Gnezdilov, Alexander Glamazda, Peter Lemmens, Kazutaka Kudo, Minoru Nohara (2025) Nanoscale Phase Separation Due to Doping and Electronic Degeneracies in Iron Pnictides, J Nanosci Technol 3(1): 101

Received Date: March 05, 2025 **Accepted Date:** April 05, 2025 **Published Date:** April 08, 2025

Abstract

We study nanoscale phase separation in iron-pnictides and its relation to doping and electronic degeneracies across the tetragonal-orthorhombic and uncollapsed to the collapsed tetragonal phases. The structural implications of these transitions are probed using the optical phonon spectrum. We notice a previously less-acknowledged coexistence of two phases on small length scales and at ambient conditions. Undoped, these phases have similar tetra-to-ortho transition temperatures. In contrast, doping leads to a cascade of phase transitions in the temperature range from 72 to 100 K. In the overdoped regime, electronic Raman scattering is observed. We attribute this to an enhancement of electronic correlations with increasing doping, leading to a non-Fermi liquid behavior. Our work shows that nanoscale phase separation in iron-pnictides can be tuned by doping leading to an unprecedented complexity which is attributed to electronic close-degeneracy and multiband physics.

Keywords: Phase separation; Correlation effects; Phase transitions; Phonon spectra

Introduction

Starting from the discovery of superconductivity in $\text{LaFeAsO}_{1-x}\text{F}_x$ with critical temperature, $T_c \approx 26$ K in 2008 [1], several families of Fe-based superconducting materials have been discovered such as 11- FeX_{1-x} ($X = \text{Se/Te/S}$), 1111- ReFeAsO ($\text{Re} = \text{La/Ce/Pr/Nd/Sm/Gd/Tb}$) [2], 111- AFeAs ($A = \text{Li/Na/La}$) [3], ternary 122- AeFe_2As_2 ($\text{Ae} = \text{Ba/Sr/Ca/Eu}$) and 122- AxFe_2Se_2 ($\text{Ax} = \text{K/Cs/Rb}$) [4], 1144- $\text{AeAFe}_4\text{As}_4$ [5], and 42622- $\text{Ae}_4\text{M}_2\text{O}_6\text{Fe}_2\text{As}_2$ ($\text{M} = \text{V/Cr/Sc}$) [6]. All iron-based superconductors consist of Fe_2X_2 ($X = \text{pnictide/chalcogenide}$) layers, which are composed of edge-sharing, distorted FeX_4 tetrahedra. Usually, these tetrahedra alternate with other intermediate layers [7] leading, e.g. to combinations of effective PtAs layers with FeAs layers [8-10]. The high interest and intensive studies of iron-based superconductors related to the interplay of multiband effects, correlation effects, and structural variations led to a rich field of physics as described in the literature (see, e.g. Refs. 11-14) that goes beyond the previously known interplay of magnetism and superconductivity modified by doping and pressure.

The 122- AeFe_2As_2 materials are among the most interesting materials in the Fe-As family of superconductors with very fragile ground states and extreme sensitivity to external pressure, annealing, and chemical doping. They are considered to be an ideal platform to study magnetic fluctuation-driven superconductivity. It was supposed that all the 122- AeFe_2As_2 compounds crystallize in the tetragonal ThCr_2Si_2 -type structure at room temperature with structural transition an orthorhombic phase at lower temperatures ($T_o \approx 171$ K for Ca [15], ≈ 205 K for Sr [16], ≈ 140 K for Ba [17], and ≈ 200 K for Eu [18]). The structural transition is accompanied by an antiferromagnetic (AFM) ordering of the Fe moments with the wave vector $Q = [1, 0, 1]$ of the spin-density-wave (SDW) pattern. Suitable substitutions on either the Ae site or the Fe site can suppress magnetic ordering, and the system becomes superconducting for certain doping ranges [19-21]. Superconductivity can also be induced by applying pressure [22].

The following general trends are reported:

i) There exist structural instabilities in 122- AeFe_2As_2 compounds related to the existence of many energy minima in their energy landscape. CaFe_2As_2 is conceivably one of the most interesting materials in the family of Fe-pnictide-based superconductors with a very fragile ground state. It combines the salient physical features of the 122- AeFe_2As_2 compounds and might serve as a model system. On the other hand, there are studies with partly contrasting results, pointing to less understood complexities inherent in these compounds. In particular, the bulk properties of CaFe_2As_2 are significantly dependent on the sample's preparation techniques (Sn flux or FeAs self-flux growth), quenching temperatures, or post-growth treatment [23].

ii) Pressure- or doping-induced isostructural (uncollapsed-tetragonal (ucT) to collapsed-tetragonal (cT)) phase transition in the 122- AeFe_2As_2 family leads to an approximately 10% shrinkage of the unit cell's c axis [24, 25]. Magnetic order as well as superconductivity is suppressed and a Fermi-liquid electronic transport is restored. Interestingly, the phase diagram of Rh^{3+} -doped CaFe_2As_2 is rather special as superconductivity occurs in a very narrow range of Rh-content ($0.020 < x < 0.024$) [26]. It occurs in between the orthorhombic AFM phase and the tetragonal nonmagnetic phase. This means that this system has probably the most intricate interplay of electronic and lattice degrees of freedom. The suppression of magnetic order can be related to an absence of a magnetic moment on the iron site, in a molecular context described by a $S = 0$ low spin state [27]. Summarizing, $\text{Ca}(\text{Fe}_{1-x}\text{Rh}_x)_2\text{As}_2$ allows in an unprecedented way to study the interplay of magnetic fluctuations, superconductivity, and the orbital or magnetic origin of the ortho-to-tetra structural phase transitions.

iii) There exists a re-entrance and competition of magnetic phases with orthorhombic C_2 and tetragonal C_4 rotational symmetry and superconductivity in the region of the superconductivity dome in the phase diagram [28-30].

Therefore, we reconsidered studying Rh^{3+} -doped $\text{Ca}(\text{Fe}_{1-x}\text{Rh}_x)_2\text{As}_2$ single crystals on freshly cleaved surfaces with an emphasis

to better understand the role of doping and phase coexistence in samples with $x = 0, 0.035,$ and 0.19 . These stoichiometries represent specific regimes of the phase diagram [26] and a focus on temperature-dependent polarized Raman spectra should lead to conclusive results. Despite the intriguing properties of undoped and doped CaFe_2As_2 , the number of spectroscopic studies is rather limited. Raman spectroscopy is a highly sensitive and informative method that allows us to reveal the local crystal distortions, defects, and impurities and to probe the phonon, electronic, and magnetic excitations simultaneously. As an example, we can cite a series of very successful fundamental Raman studies on the spin and charge degrees of freedom in iron-containing pnictides and chalcogenides [31].

The performed data analysis indicates that in the undoped CaFe_2As_2 sample, four modes instead of the two symmetry-allowed ones are observed. They are pairs of A_{1g} and B_{1g} modes that give evidence for the presence of two tetragonal phases in the sample. This suggests a phase separation into tetragonal uncollapsed and collapsed phases in undoped CaFe_2As_2 at ambient conditions. Evidence for such a phase separation or structural modulations on small length scales have been found before and will be discussed in detail. Both phases undergo a tetra-to-ortho structural phase transition under cooling. Within the accuracy of our technique, the transition temperatures of these phases are similar.

For the $x = 0.035$ sample, we also observed spectra corresponding to two phases at room temperature. However, up to $T = 100$ K, we did not observe the appearance of all four lines in the YX -scattering geometry. Below some critical $T^* \approx 100$ K, we observe the emergence of new phonon lines in coexistence with the previous ones. The only explanation for this feature is the emergence of a new order parameter with different translation symmetry. Upon further cooling to the temperature of the uncollapsed \rightarrow collapsed tetragonal phase transition T_{cT} , cardinal changes occur in the Raman spectra. One can suppose that the last effect is related to the remnant magnetic ordering which should be realized in the uncollapsed phase of the phase-separated $x = 0.035$ sample with iron atoms in a nonzero spin state.

The overdoped sample with $x = 0.19$ located on the right side of the phase diagram [26] of $\text{Ca}(\text{Fe}_{1-x}\text{Rh}_x)_2\text{As}_2$ also shows phase separation in the temperature range of $7 - 295$ K.

In addition, $\text{Ca}(\text{Fe}_{1-x}\text{Rh}_x)_2\text{As}_2$ is considered as an unconventional superconductor, which cannot be described according to the Bardeen-Cooper-Schrieffer theory and mean-field electron-phonon coupling. In particular, nanoscale phase separation with delicate sublattice interactions revealed in our Raman studies may play an important role in the emergence of the superconducting state in a surprisingly narrow Rh^{3+} doping range.

Materials and Methods

Single crystals of $\text{Ca}(\text{Fe}_{1-x}\text{Rh}_x)_2\text{As}_2$ ($x = 0, 0.035,$ and 0.19) were grown using a self-flux method. Details of the growth of single crystals and the resulting phase diagram are given in Ref. 26 (Figure S1 in Supplementary Information). In addition, X-ray diffraction experiments have been performed after the Raman study to ensure their structural integrity. The freshly cleaved samples were installed into a He-closed cycle cryostat (Oxford/Cryomech Optistat) with a temperature-controlled range of $T = 7 - 295$ K. Raman-scattering experiments were performed in quasi-backscattering geometry using a $\lambda = 532$ nm solid-state laser. The laser power was set to 7 mW with a spot diameter of approximately $100 \mu\text{m}$ to avoid heating effects. The local heating in the laser spot didn't exceed 1 K. The spectra were collected via a triple spectrometer (Dilor-XY-500) by a liquid-nitrogen-cooled CCD (Horiba Jobin Yvon, Spectrum One CCD-3000V).

Raman spectra were measured in parallel and crossed scattering geometry with X and Y laboratory axes rotated at 45 degrees relative to the crystallographic a and b axes (see the inset of Figure 1). This choice and additional details are discussed in the Supplementary Information. The spectra were fitted using sets of Lorentz functions.

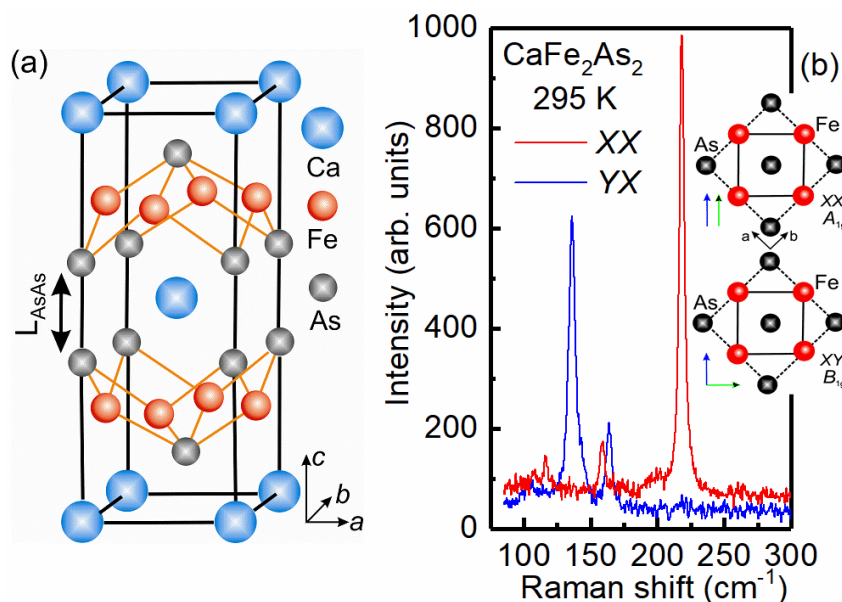


Figure 1: (a) The crystal structure of CaFe₂As₂ at ambient conditions. (b) Room temperature Raman spectra of the CaFe₂As₂ single crystal measured from the ab plane in two scattering geometries. The inset on the right shows the scattering geometry used in the experiment with the directions of the incoming (blue arrows) and scattered (green arrows) photon polarizations rotated by 45 degrees relative to the *a* and *b* axes of the crystal.

Results and Discussion

Undoped $x = 0$ samples. CaFe₂As₂ at ambient pressure and temperature realizes the paramagnetic tetragonal ThCr₂Si₂-type structure (space group $I4/mmm$ (D_{4h}^{17} , #139) with lattice parameters $a = 3.887(4)$ Å, $c = 11.758(23)$ Å [32]. The crystal structure of CaFe₂As₂ under ambient conditions is shown in Figure 1.a. Alkaline-earth ions, Fe, and As occupy 2a, 4d, and 4e positions, respectively. According to the factor group analysis for the $I4/mmm$ space group, the total irreducible representation of Raman-active phonon modes is given by four Raman-active phonons: A_{1g} (As), B_{1g} (Fe), E_g (As), and E_g (Fe), see also the Supplementary Information.

Upon cooling at ambient pressure, CaFe₂As₂ undergoes a first order transition at about 170 K from the high temperature tetragonal-paramagnetic phase into the low temperature orthorhombic structure (space group $Fmmm$ (D_{2h}^{23} , #69)). It is accompanied by the appearance of a spin density wave (SDW) state, which has been observed in a variety of experiments [33]. This tetragonal-to-orthorhombic (T-O) structural phase transition in a parent, as well as substituted, CaFe₂As₂ is extremely sensitive to external stresses and strains and can be even partially or completely suppressed. The factor group analysis of low-temperature $Fmmm$ phase with Ca, Fe, and As in 4a, 8f, and 8i Wyckoff positions, respectively yields six Raman-active phonon modes: $\Gamma_{\text{vib}} = A_g(\text{As}) + B_{1g}(\text{Fe}) + 2B_{2g}(\text{As,Fe}) + 2B_{3g}(\text{As,Fe})$.

In a Raman study by K.-Y. Choi et al. [34] two weak phonon modes were observed at 182 (189) cm⁻¹ - A_{1g} and 204 (211) cm⁻¹ - B_{1g} at $T = 295$ and 4 K, respectively. The authors also noted abrupt changes in the temperature-dependence of the frequencies and linewidths upon cooling down through the first-order $I4/mmm \rightarrow Fmmm$ structural phase transition near 170 K. In a second study by Kumar and co-workers, three phonon modes were observed in electron-doped single crystals, Ca(Fe_{0.95}Co_{0.05})₂As₂ [35]. They were assigned to the 205 cm⁻¹ - B_{1g} : Fe, 215 cm⁻¹ - A_{1g} : As, and 267 cm⁻¹ - E_g : Fe and As modes and displacements. These modes showed anomalies at the tetragonal-to-orthorhombic structural transition at $T_O \approx 140$ K.

We performed shell-model calculations of the CaFe₂As₂ lattice dynamics [36] taking model parameters for Fe²⁺, Ae²⁺, and As³⁻

ions from Ref. 37 as starting points. For homogeneous CaFe_2As_2 , we obtained the A_{1g} and B_{1g} modes frequencies 182 and 201 cm^{-1} , in good agreement with the experimental Raman data.

Our room temperature Raman spectra of single crystalline CaFe_2As_2 measured from the ab plane are shown in Figure 1.b. The sharpness and large scattering intensity of the observed peaks are related to the high quality of the studied single crystals. These data show four well-resolved phonons. The extracted frequencies of the Raman-active optical phonon modes are the two A_{1g} (159 and 218 cm^{-1}) and B_{1g} (136 and 164 cm^{-1}) modes, respectively. A weak $E_g(\text{Fe,As})$ at around 116 cm^{-1} is observed and assigned to a small leakage due to the quasi-backscattering geometry of the experiment. Similar data were achieved on different sample batches. The assignment of the observed modes has been performed based on the shell lattice calculations mentioned above and Raman tensors resolved from the Bilbao Crystallographic Server [38]. Furthermore, we state that the frequency of the most intensive 218 cm^{-1} $A_{1g}(\text{As})$ mode is higher compared to the frequencies of both $B_{1g}(\text{Fe})$ modes (which should be the other way around, given the As and Fe ions mass ratio). Summarizing, the present phonon spectra are more complex than the ones previously reported [34, 35, 37].

The observation of two pairs of Raman modes is evidence for two tetragonal phases in the single crystal. Assuming that the ratio of the mode intensities corresponds to the volume ratio of the phases, it is reasonable to assign the 218 $\text{cm}^{-1}(A_{1g})$ and 136 $\text{cm}^{-1}(B_{1g})$ to the t1 tetragonal phase and the second pair of modes of 159 $\text{cm}^{-1}(A_{1g})$ and 164 $\text{cm}^{-1}(B_{1g})$ - to the t2 tetragonal phase. With this identification, the frequency order of A_{1g} and B_{1g} modes in phase t2 is identical to the one previously observed and calculated [34, 37].

Our observation agrees also well with the complex phase diagram of CaFe_2As_2 [39-44]. Accordingly, undoped CaFe_2As_2 can be stabilized in two slightly different tetragonal phases (PI and PII) by rapid quenching from 850 °C and prolonged annealing at 350 °C, respectively. The PI phase with lattice parameter $c = 11.547(1)$ Å corresponds to a tetragonal structure at room temperature and transforms to a cT phase with $c = 10.720(1)$ Å below the T-cT transition temperature $T_{cT} \approx 100$ K. The PII phase also exhibits a tetragonal structure at room temperature but with a slightly longer c ($c = 11.763(1)$ Å). It undergoes a tetragonal--to-orthorhombic (T-O) structural transition at $T_O \approx 170$ K. It was found that the PI and PII phases could be reversibly transformed through PI + PII-mixing phases by a heat treatment [43]. This supports our assignment of the mode multiplication to a coexistence of phases.

Various research techniques were used to identify and better understand phase separation in CaFe_2As_2 and its dependence on various heat treatment procedures [39, 44-46]. Systematic XRD and HRTEM studies found related micro- and nanoscale structures and their evolution with annealing CaFe_2As_2 [45]. They revealed the presence of a clear pseudo-periodic structural modulation at room temperature with a wavelength of around 40 nm, interpreted as local structural distortions within the Ca layers [45].

Also, angle-resolved photoemission spectroscopy CaFe_2As_2 [47] found related features. They revealed a hitherto hidden cT phase in CaFe_2As_2 under ambient conditions, which were attributed to quantum fluctuations and exotic electronic properties. Similar conclusions were based on hard X-ray photoemission spectroscopy [48]. Annealing leads to an increasing transition temperature of the antiferromagnetic phase transition. For the most homogeneous crystals, the antiferromagnetic and orthorhombic phase transitions occur at 168 K [39]. This confirms our results with similar transition temperature of the two phases.

The effect of magnetic ordering on the phonon system has previously been studied in CaFe_2As_2 and $\text{Ca}(\text{Fe,Co})_2\text{As}_2$ [35]. A strong spin-phonon coupling has been found with frequency shifts of the order of 20 – 50 cm^{-1} from the paramagnetic to antiferromagnetic phases. This is in good agreement with our observations for the t1 phase, with an inversion of the $A_{1g}(\text{As})$ mode

with respect to the $B_{1g}(\text{Fe})$ mode.

Such large effects can also be described in terms of changing 3d electron occupation named Fe-spin state that modulates the interactions of the As ions as well as shifts the c axis lattice parameter [49]. Decreasing the Fe-spin state reduces the Fe-As bonding, which leads to an increase in the As-As bonding and causes the observed huge reduction in lattice parameters. It is noted that this effect is maximal in the case of the CaFe_2As_2 system due to the proximity of two arsenic ions in adjacent Fe-planes. Similar effects have been stated for the FeTe compounds [50].

The evolution of XX and YX Raman spectra of undoped CaFe_2As_2 with temperature are shown in Figure 2. Upon cooling, the main effects of the $I4/mmm \rightarrow Fmmm$ structural transition should be a splitting of the E_g modes and Raman tensor transformation. Indeed, we observe such effects during the structural T-O phase transition at $T_o = 160$ K of both tetragonal phases in CaFe_2As_2 . The low-frequency modes at $100\text{-}130\text{ cm}^{-1}$ can be assigned with either B_{2g} or B_{3g} . This is of secondary importance and not further discussed here.

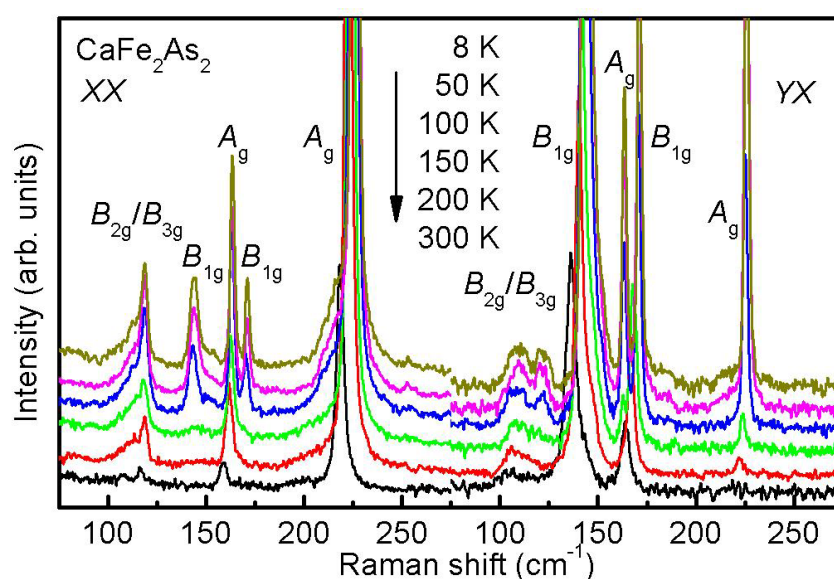


Figure 2: Temperature dependent Raman spectra of the CaFe_2As_2 single crystals measured from the ab plane in two scattering geometries. The spectra are vertically shifted for clarity. Splitting are attributed to the structural T-O phase transition at $T_o = 160$ K of both tetragonal phases.

Figures 3.a and 3.c show the respective analysis of phonon frequencies. Upon lowering temperature all phonon modes show a weak anomaly at about $T_o = 160$ K adding to the standard anharmonicity [51].

In Figures 3.b and 3.d the integrated phonon intensities of the Raman active modes are given. There exists a change in slope and a significant enhancement of the intensity of the $A_{1g}(\text{As})$ and $B_{1g}(\text{Fe})$ modes belonging to the t1 phase with crossing T_o upon cooling. The Raman intensity of a phonon mode consists of the scattering volume multiplied by the electronic polarizability of the respective displacement. As the scattering volume and optical penetration depth develop in parallel for the t1 and t2 phases, the anomalies must be related to the local enhancement of electronic polarizability in the t1 phase. We relate this to an electronic and structural instability [52] found in resistivity measurements in CaFe_2As_2 [39].

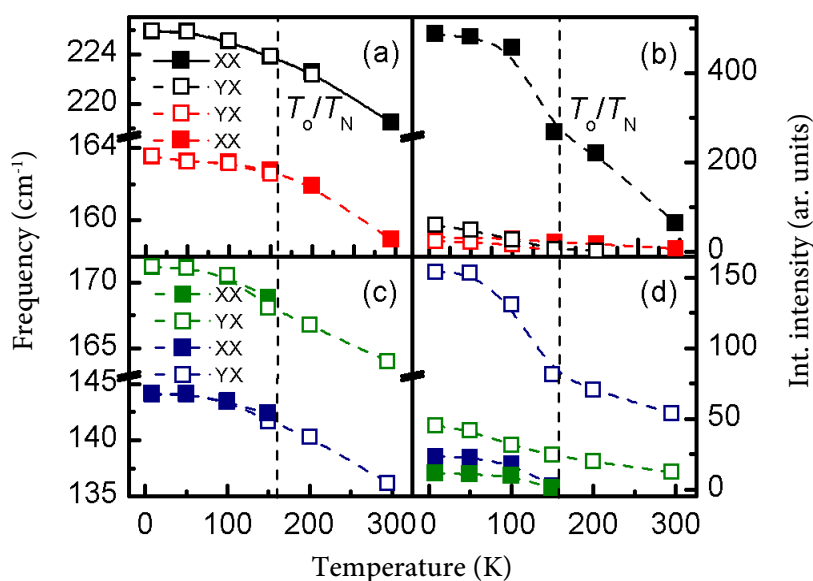


Figure 3: (a,c) Temperature dependencies of the frequency peak positions and (b,d) integrated intensities of the Raman active phonon modes in undoped CaFe_2As_2 .

Summarizing the above we see evidence for phase separation into two tetragonal phases even in the parent CaFe_2As_2 . These phases may very well consist of the tetragonal collapsed and uncollapsed phases. However, also modulations of the Ca planes or ordering processes along the c axis have been proposed based on structural investigation. Both phases undergo a tetra-to-ortho structural phase transition under cooling as shown by the appearance of phonon modes simultaneously in XX and YX-scattering geometries. Within our accuracy, the transition temperatures of the tetra-to-ortho transition are the same for both phases. This could be related to the existence of magnetic moments in both phases or due to the crosstalk of a nonmagnetic cT phase due to the surrounding magnetic ucT phase.

Doped $x = 0.035$ sample. This sample is on the verge of the orthorhombic AFM phase and the tetragonal nonmagnetic phase of $\text{Ca}(\text{Fe}_{1-x}\text{Rh}_x)_2\text{As}_2$ [26]. Figure 4 shows the temperature-dependent evolution of polarized Raman spectra of the $x = 0.035$ single crystal. The number of strong phonon lines and their frequencies are similar to those of the undoped sample (Figure 2). So, the same two-phase separation scenario is suggested. It should be noted that small orthorhombic distortions are already present in the tetragonal phase t1 at room temperature as there exist low-intensity $A_{1g}(\text{As})$ and $B_{1g}(\text{Fe})$ lines in the forbidden scattering geometries. This could be an internal pressure effect induced by the Rh doping. However, cooling down to $T^* \approx 100$ K, no change is observed.

Below the critical temperature T^* , we observe the appearance of a number of new phonon lines (see Figures 4 and 5). This T -dependence completely excludes a Rh-impurity origin of the new lines. To ensure that these “unusual” observations are not connected to an electronic resonance effect, we carried out Raman measurements using different excitation energies. Our data (see Figure 6) unequivocally rule out the presence of resonance effects. It is clearly seen that Raman spectra measured at different laser excitations practically coincide.

The temperature dependence of these modes (see Figure 7, with magnetic susceptibility from Ref. 26) indicates that there is an intermediate region about 28 K wide between T^* and T_{CT} . Please note that the observation of the coexistence of several phases in the temperature range of 45 K to 90 K in Ref. 39 is very probably related to strain fields and the formation of domains of varying c lattice parameters. Our data does not show such anomalies.

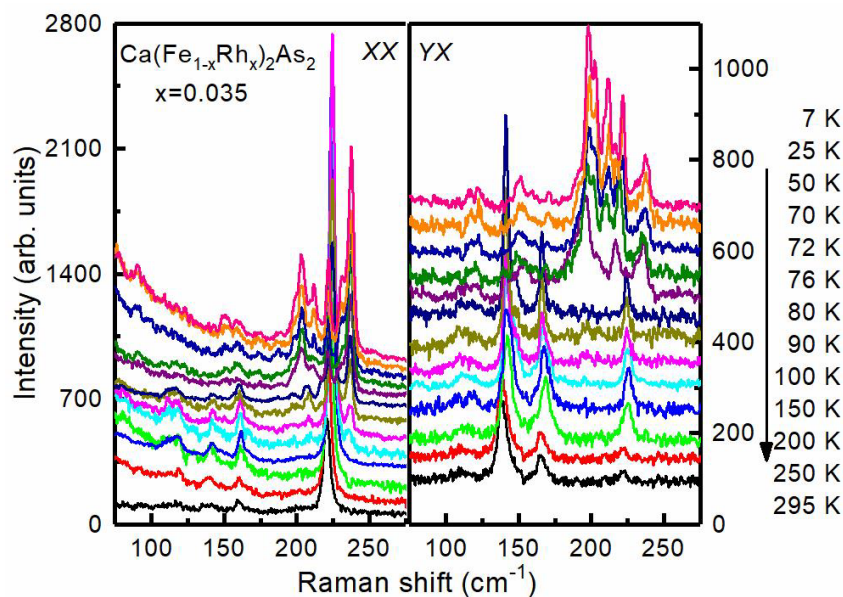


Figure 4: Temperature dependent XX and YX Raman spectra of $\text{Ca}(\text{Fe}_{1-x}\text{Rh}_x)_2\text{As}_2$, $x = 0.035$.

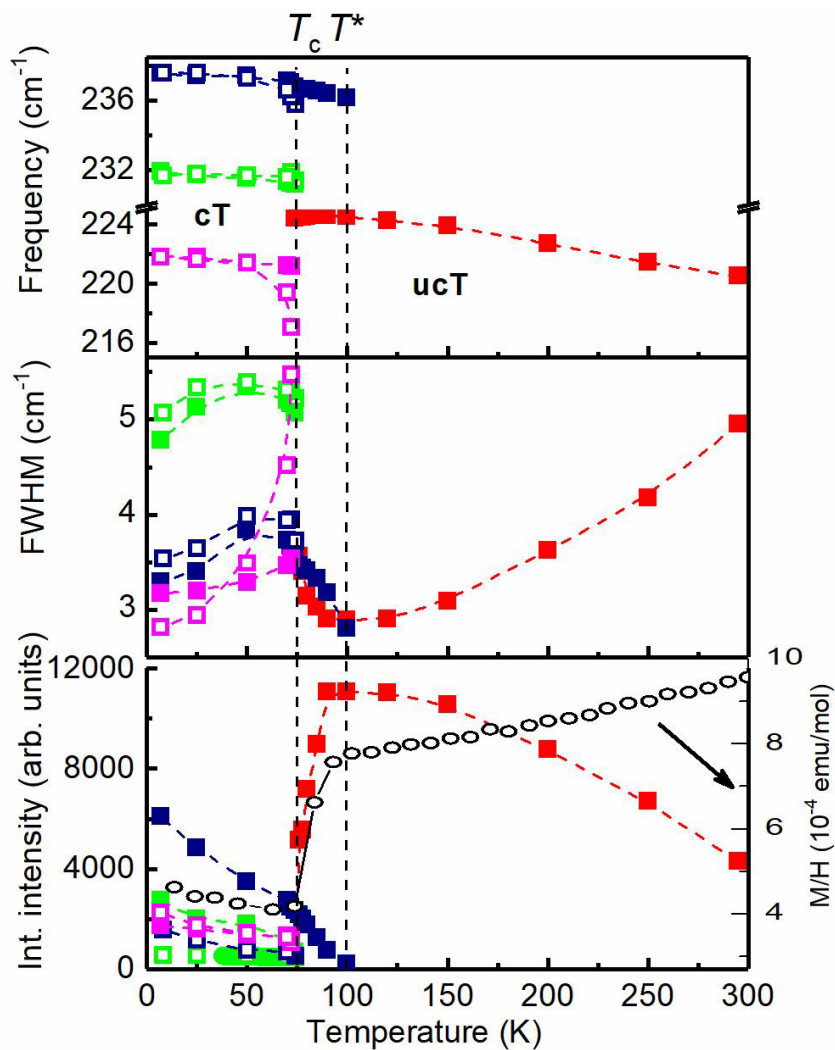


Figure 5: Temperature dependence of the phonon lines' parameters (frequency, linewidth (FWHM), and integrated intensity) of $\text{Ca}(\text{Fe}_{0.965}\text{Rh}_{0.035})_2\text{As}_2$ in the frequency region of $215 - 240 \text{ cm}^{-1}$ together with the temperature dependence of magnetic susceptibility, M/H [26].

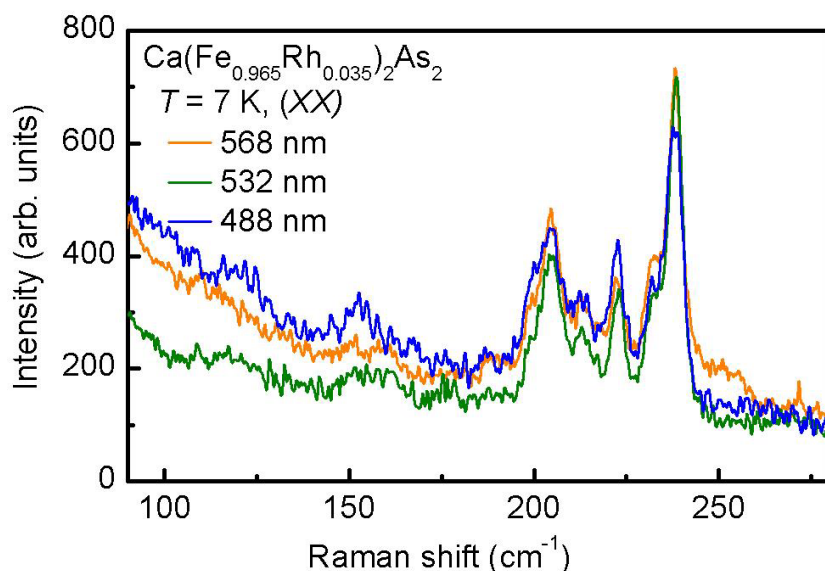


Figure 6: Raman spectra of $\text{Ca}(\text{Fe}_{1-x}\text{Rh}_x)_2\text{As}_2$, $x = 0.035$, with three different excitation wavelengths

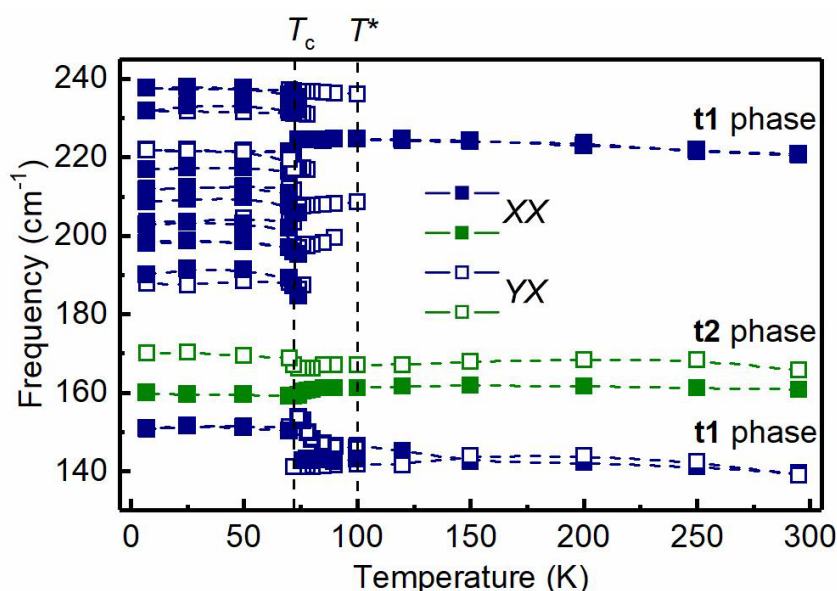


Figure 7: Overview of the phonon modes in the frequency range of $130 - 245 \text{ cm}^{-1}$ as function of temperature for $x = 0.035$ in XX and YX scattering geometries

With cooling below $T_{cT} = 72 \text{ K}$ we notice a large frequency shift of the A_{1g} (161 cm^{-1}) and B_{1g} (167 cm^{-1}) lines for temperatures below the temperature T_{cT} of $\text{ucT} \rightarrow \text{cT}$ phase transition. As for the t1 phase, the phonon Raman spectra at low temperatures change completely. The phonon lines of the uncollapsed tetragonal phase fully disappear and new lines appear. Moreover, below T_{cT} all phonon lines are active in both parallel and crossed scattering geometries. Regarding earlier X-ray and neutron scattering experiments, and nonmagnetic DFT calculations [25] this is a surprising result. In the latter only smaller effects are expected through the uncollapsed \rightarrow collapsed tetragonal phase transition. In contrast, changes in the spectra of the t2 phase are in good agreement with Ref. 25. We attribute this to the emergence of a new order parameter with translational degrees of freedom.

Unconventional high- T_c superconductivity in iron pnictides is related to Fe-magnetism. The competition of superconductivity and magnetism is especially pronounced in the re-entrance of the SDW phases C_2 (twofold) and C_4 (fourfold rotational) symmetry inside the superconducting dome both in electron- [28] and hole-doped [29, 30] AeFe_2As_2 . Numerous studies showed (see,

e.g. Ref. 49) that Fe-magnetism is not totally lost in the cT-phase, but it is only partially reduced. Different mechanisms, namely, magnetic and orbital ordering, for symmetry lowering in the orthorhombic and the re-entrant tetragonal phases were considered in the hole-doped $\text{Ba}_{0.76}\text{Na}_{0.24}\text{Fe}_2\text{As}_2$ [53]. However, in this compound, the transition is not complete and the re-entrant phase coexists with the orthorhombic down to the lowest measured temperature of 1.5 K. The magnetic mechanism for symmetry lowering in the re-entrant tetragonal phase with out-of-plane magnetic moments implies a two- k magnetic structure with tetragonal P_4A_2/ncm symmetry which imposes zero dipole magnetic moments for half of the Fe sites. In this case, the crystal structure symmetry (ignoring the magnetic subsystem) of the system is well approximated by the parent $I4/mmm$ space group. The orbital ordering mechanism predicts a lowering of symmetry down to $P4/mnc$ or $I422$ depending on the stacking of the (ab) ordered layers along the c axis. Both types of orbital ordering do not allow any atomic displacements in comparison with the parent $I4/mmm$ space group. The combination of the magnetic order with orbital M_3^+/Γ_1^- ordering results in the orthorhombic $P_c ccn/C_A 222_1$ magnetic space groups, respectively.

The most preferable magnetic structure of $\text{Ba}_{0.76}\text{Na}_{0.24}\text{Fe}_2\text{As}_2$ in the re-entrant phase according to Ref. 53 is the tetragonal one, P_4A_2/ncm , with G-type order of nonmagnetic and magnetic states on neighboring iron atoms (see Figure 4 in Ref. 53). Such a structure should lead to the appearance of a number of new phonon modes in Raman scattering. Nevertheless, with a high probability, we can assert a novel re-entrance of the C_2 -symmetric phase in $x = 0.035$ doped sample at $T < 72$ K that coexists with the collapsed tetragonal phase. The last statement is based on the fact that: i) there exist only insignificant orthorhombic distortions evidenced from Raman scattering; ii) at temperatures below $T_c = 72$ K, all appeared phonon excitations are active in both parallel and perpendicular scattering geometries. Note that these new phonon modes are not present in the magnetically ordered uniform phase of the $x = 0$ undoped sample. This evidences that its magnetic structure is distinct from the orthorhombic one at low temperatures with $x = 0.035$. For a further discussion, we refer to Ref. 53.

Overdoped $x = 0.19$ sample. This sample is located on the right side of the electronic phase diagram of $\text{Ca}(\text{Fe}_{1-x}\text{Rh}_x)_2\text{As}_2$ with a first-order phase transition from the ucT phase to the cT at comparably high temperatures, i.e. $T_{cT} = 295$ K [26]. Respective Raman spectra at 295 and 420 K in Figure 8 show very weak phonon lines and a pronounced quasielastic scattering. The latter is assigned to electronic Raman scattering due to the enhanced charge carrier concentration with Rh-doping. Such electronic scattering is rarely observed in conventional metals due to screening. In the present case, non-Fermi liquid behavior evidenced from electronic transport reduces screening in a scenario similar to cuprate HTSC. Subtracting the electronic contribution leads to the spectrum shown in the inset of Figure 8. We notice the appearance of additional bands in the frequency region of high (245 cm^{-1}) and low (165 cm^{-1}) energy phonons probably related to impurities. Such impurities are often observed in layered materials.

In Figure 9 we compare spectra with $x = 0.035$ and $x = 0.19$ at $T = 70$ K and 295 K, respectively. We notice for $x = 0.19$ that there exist broadened phonon lines at Room temperature in the same frequency region where the $x = 0.035$ sample in the cT phase indicates phase separation with intensive, multiplied phonon lines. This indicates that the $x = 0.19$ sample shows a similar phase separation at high temperatures that exists for $x = 0.035$ only at $T < T_c$.

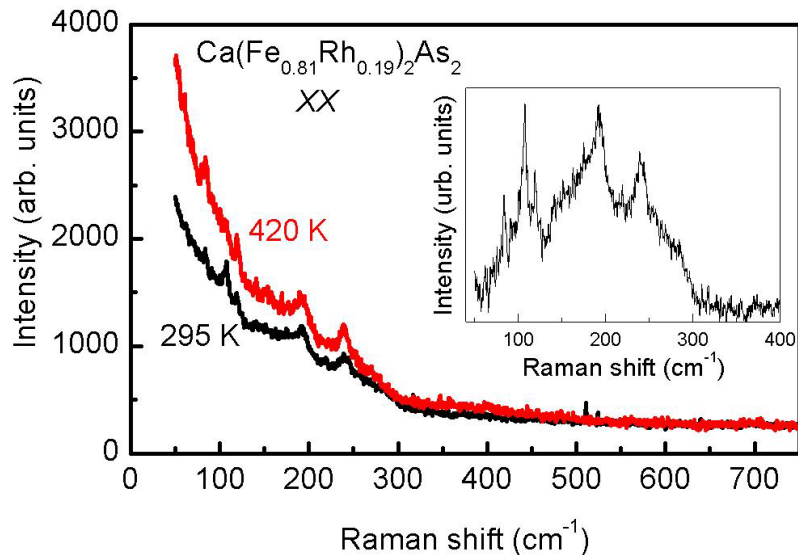


Figure 8: Raman spectra of the overdoped single crystal $\text{Ca}(\text{Fe}_{1-x}\text{Rh}_x)_2\text{As}_2$, $x = 0.19$, from the ab plane in XX scattering geometry at 295 and 420 K. The inset shows a spectrum at $T = 295$ K with a subtracted quasielastic background of electronic origin.

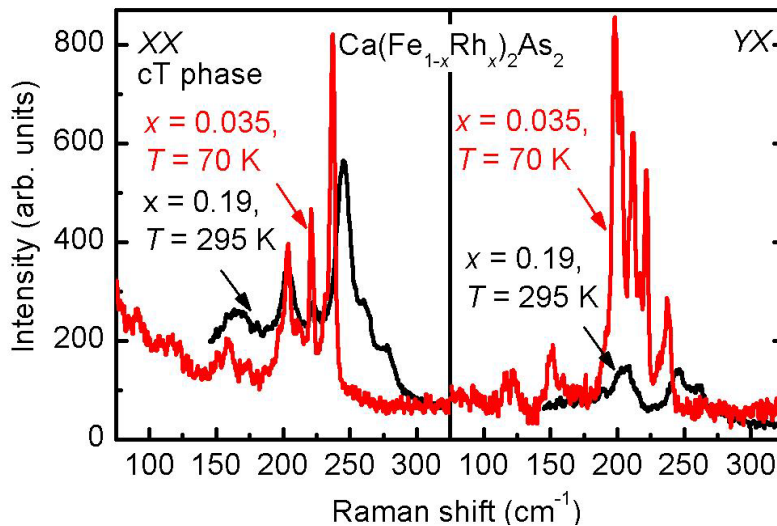


Figure 9: Comparison of Raman spectra of $x = 0.19$ at room temperature with 70 K-spectra of $x = 0.035$ in the cT phase. Data are from the ab plane and in the XX and YX polarization, respectively.

Thus, our Raman studies have made it possible to very clearly demonstrate the tendency of the $\text{Ca}(\text{Fe}_{1-x}\text{Rh}_x)_2\text{As}_2$ system to microstructural phase separation, a property that was not expected in this material, gives rise to discussion and requires further study. Besides, for the first time, structural-phase transformations were detected in the doped samples during the transition to a collapsed state, which contradicts the statements of previous studies using various experimental methods.

Conclusions

Fe-based superconductors are distinct from other high temperature superconductors with respect to specific features of the Fe ion itself, related multiband effects, degeneracies, and electronic crossover phenomena. In particular, $\text{Ca}(\text{Fe}_{1-x}\text{Rh}_x)_2\text{As}_2$ has a phase diagram with a very restricted regime of superconductivity, evidence for structural modulations, and phase separation that are affected by thermal annealing procedures close to room temperature. Therefore, a careful reinvestigation of Raman scattering spectra with the special emphasis on phase separation is desirable.

In detail, we have observed evidence for nanoscale phase separation for both the undoped ($x = 0$) and the doped ($x = 0.035$) samples. It is most reasonable to attribute these phases to the collapsed and uncollapsed tetragonal phases with slightly different volumes of the unit cells. However, previous studies using TEM and X-ray diffraction found evidence for modulation effects in the Ca planes and the c axis parameters that are not described within this scenario. Analyzing the resolved scattering intensities of the Raman experiments it follows that these phases are not limited to local distortions.

Further experiments show that the observed transition temperatures of the two phases coincide within a few K. This could be based on an intrinsic effect or follow a scenario of mutual interaction of the order parameters in the two phases. We suggest that the cT and ucT phases should possess similar magnetic moments.

With cooling from room temperature to below $T^* \approx 100$ K new phonon lines emerge in the spectra and with decreasing temperatures through the ucT–cT transition temperature, $T_{cT} = 72$ K [26], drastic changes occur in the spectra. For the intermediate temperature interval, we propose a structural distortion that precedes the transition from the uncollapsed to the collapsed tetragonal phase transition. Interestingly a similar scenario has been discovered in $\text{Ba}_{1-x}\text{Na}_x\text{Fe}_2\text{As}_2$ ($x = 0.24 - 0.28$) based on resonant X-ray scattering [53]. In the overdoped sample ($x = 0.19$) [26] observation of electronic Raman scattering points to the importance of non-Fermi liquid behavior as also evidenced by electric transport.

Summarizing, our study of optical phonons thought the phase diagram of $\text{Ca}(\text{Fe}_{1-x}\text{Rh}_x)_2\text{As}_2$ shows a surprising complexity as well as phase separation that goes beyond previous studies. In light of similar effects in other classes of layered materials, such as the Kitaev material $\alpha\text{-RuCl}_3$ and transition metal dichalcogenides, it might be important to reconsider the interplay of electronic degeneracies with local and collective distortions. Such studies may lead to an improved and deeper material understanding, beyond basic structural studies and conventional electron-phonon coupling. In this sense we have opened an avenue that did not show up in other physical methods [55] with Raman spectroscopy being a highly sensitive probe of local variations of polarizability.

Acknowledgments

V.G. and A.G. thank the Nanophotonics journal, De Gruyter, Sciencewise Publishing, and the Optica Foundation for a financial support through the Ukraine Optics and Photonics Researcher Grants. A.G. gratefully thanks Dr. A. Peschanskii and Dr. N. Galtsov (B. Verkin Institute for Low Temperature Physics and Engineering of the National Academy of Sciences of Ukraine) for the interest in the presented work and the valuable discussions. We acknowledge support by EXC-2123 Quantum Frontiers–390837967, DFG-Nanomet, and Grants-in-Aid for Scientific Research (JP19H05823, JP22H01182, JP23K22453, JP24K21531, JP23H04630, JP23H04861) provided by the Japan Society for the Promotion of Science

Author Contributions

V. Gnezdilov: Conceptualization, Spectroscopic analysis, Writing - review & editing. A. Glamazda: Formal analysis, Conceptualization. Peter Lemmens: Writing, review & editing, conceptualization, Resources, Project administration, Funding acquisition. K. Kudo: Methodology, Formal analysis. M. Nohara: Methodology, Formal analysis.

Data Availability

Data sets generated during the current study are available from the corresponding author on reasonable request. The additional information on the scattering geometry, chemical composition of the samples, and X-ray analysis is included in the Supplementary Information file.

Declaration

Conflicts of Interests

The authors do not have any commercial or associative interest that represents any conflict of interest in connection with the work submitted.

Supplementary Information

Here we discuss the scattering geometry used in the Raman studies of pure and Rh-doped CaFe_2As_2 single crystals, see also the inset in Fig. 1. The factor group analysis yields four Raman-active phonon modes for CaFe_2As_2 (space group $I4/mmm$), $\Gamma_{\text{Raman}} = A_{1g}(x^2 + y^2, z^2) + B_{1g}(x^2 - y^2) + 2E_g(xz, yz)$.

The corresponding Raman tensors are given by the following matrices [1]:

$$A_{1g} \rightarrow \begin{pmatrix} a & 0 & 0 \\ 0 & a & 0 \\ 0 & 0 & b \end{pmatrix}, B_{1g} \rightarrow \begin{pmatrix} c & 0 & 0 \\ 0 & -c & 0 \\ 0 & 0 & 0 \end{pmatrix}, E_{g_1}, E_{g_2} \rightarrow \begin{pmatrix} 0 & 0 & -e \\ 0 & 0 & 0 \\ -e & 0 & 0 \end{pmatrix}, \begin{pmatrix} 0 & 0 & 0 \\ 0 & 0 & e \\ e & 0 & 0 \end{pmatrix}.$$

Using the polarization selection rules and the fact that only the ab plane can be prepared by controlled cleaving processes, the assignments of the modes is straightforward. In particular, the A_{1g} and B_{1g} modes are observed in the parallel and crossed scattering geometries with the laboratory axes X, Y parallel to the a, b axis of the crystal respectively. At a 45 degree rotation of the sample, the Raman tensors transform to [1]:

$$A_{1g} \rightarrow \begin{pmatrix} a' & 0 & 0 \\ 0 & a' & 0 \\ 0 & 0 & b \end{pmatrix}, B_{1g} \rightarrow \begin{pmatrix} 0 & c' & 0 \\ c' & 0 & 0 \\ 0 & 0 & 0 \end{pmatrix}, E_{g_1}, E_{g_2} \rightarrow \begin{pmatrix} 0 & 0 & g' \\ 0 & 0 & g' \\ g' & g' & 0 \end{pmatrix}, \begin{pmatrix} 0 & 0 & f' \\ 0 & 0 & g' \\ f' & g' & 0 \end{pmatrix}.$$

The surfaces of high- T_c iron-containing superconductor samples are not stable against surface oxidation. Therefore, freshly cleaving the surfaces is mandatory which restricts the number of scattering geometries, see inset of Fig. 1b. In the latter A_{1g} and B_{1g} modes may be investigated separately in one sample setup.

Below in Fig. S1 we present the electron phase diagram of $\text{Ca}(\text{Fe}_{1-x}\text{Rh}_x)_2\text{As}_2$ with $0.00 \leq x \leq 0.22$, adapted from Ref. 2, where the yellow arrows show the Rh-concentrations of the samples we studied.

We performed repeated X-ray analysis on the single crystals from different growth batches (see Fig. S2). The new data showed an excellent agreement with initial experiments. However, the XRD did not show a sufficient sensitivity to recover the nanoscale phase separation. This may also be due to the higher sensitivity of Raman scattering with respect to bond distortions and other phenomena, see, e.g. [3].

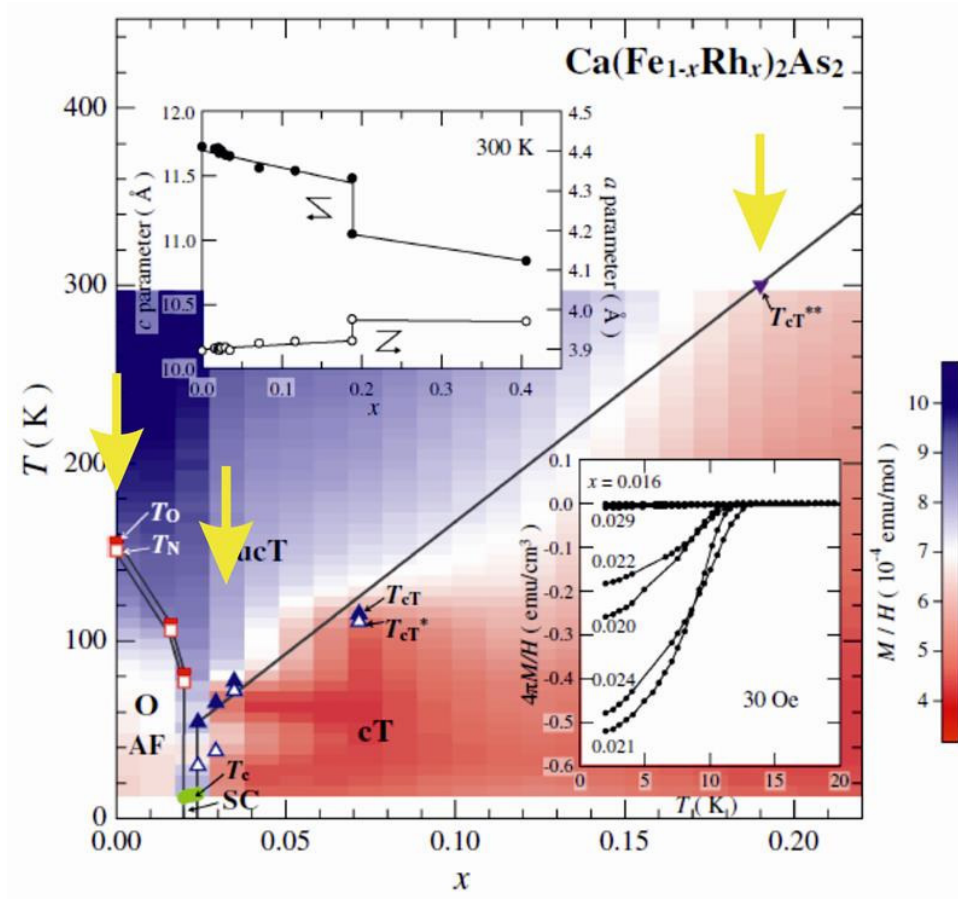


Figure S1: The electronic phase diagram of $\text{Ca}(\text{Fe}_{1-x}\text{Rh}_x)_2\text{As}_2$. O, ucT, and cT denote the orthorhombic, uncollapsed-tetragonal, and collapsed-tetragonal structure, respectively. Plot adapted from Ref. [2]. SC and AF denote the superconducting and the antiferromagnetically ordered phases, respectively. T_c , T_o , and T_n are the superconducting, ucT-O, and AF transition temperatures, respectively.

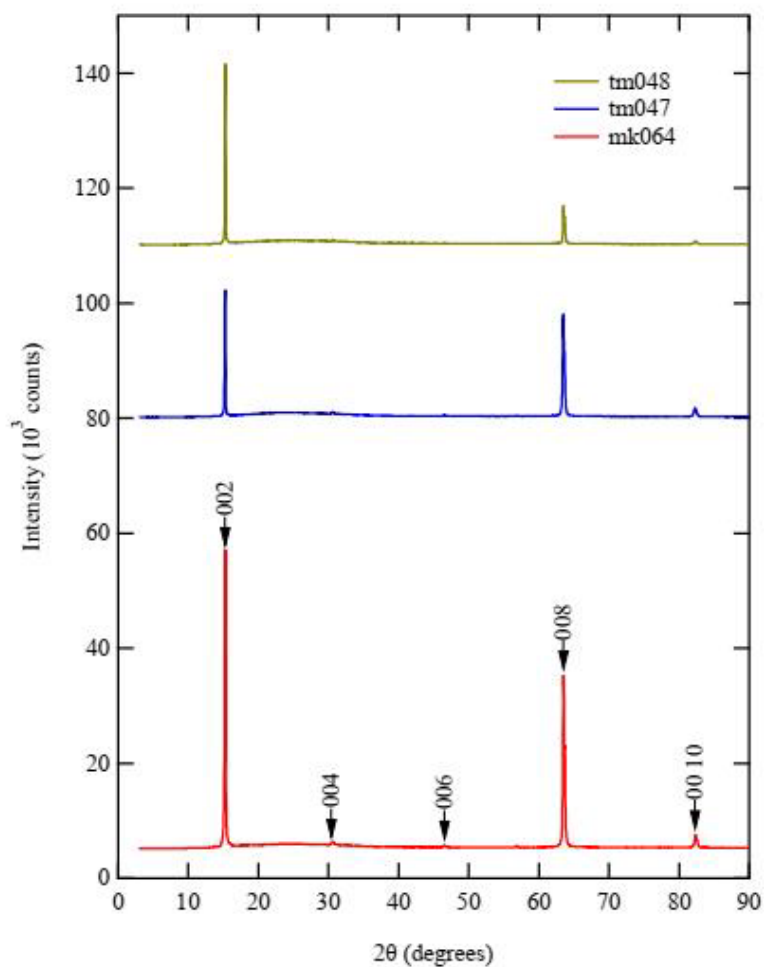


Figure S2: XRD patterns for CaFe₂As₂ single crystals from different growth batches at 300 K.

References

1. Kroumova E, Aroyo MI, Perez-Mato JM, et al. (2003) Bilbao Crystallographic Server: Useful Databases and Tools for Phase-Transition Studies. *Phase Transitions: A Multinational Journal*, 76:155-170.
2. Danura M, Kudo K, Oshiro Y, et al. (2011) Interplay of Superconductivity and Fermi-Liquid Transport in Rh-Doped CaFe₂As₂ with Lattice-Collapse Transition. *J Phys Soc Jpn*, 80:103701.
3. Wang CP, Shieh SR, Withers AC, et al. (2020) Raman and X-ray diffraction study of pressure-induced phase transition in synthetic Mg₂TiO₄. *Sci Rep*, 10:6278.

References

1. Kamihara Y, Watanabe T, Hirano M, Hosono H (2008) Iron-Based Layered Superconductor $\text{La}[\text{O}_{1-x}\text{F}_x]\text{FeAs}$ ($x = 0.05\text{--}0.12$) with $T_c = 26$ K. *J Am Chem Soc*, 130:3296-7.
2. Chen X, Wu T, Wu G, et al. (2008) Superconductivity at 43 K in $\text{SmFeAsO}_{1-x}\text{F}_x$. *Nature* 453:761-2. And Chen GF, Li Z, Wu D, et al. (2008) Superconductivity at 41 K and Its Competition with Spin-Density-Wave Instability in Layered $\text{CeO}_{1-x}\text{F}_x\text{FeAs}$. *Phys Rev Lett*. 100:247002. And Wen HH, Mu G, Fang L, et al. (2008) Superconductivity at 25 K in hole-doped $(\text{La}_{1-x}\text{Sr}_x)\text{OFeAs}$. *EPL*. 82:17009. And Ren ZA, Yang J, Lu W, et al. (2008) Superconductivity at 55 K in Iron-Based F-Doped Layered Quaternary Compound $\text{Sm}[\text{O}_{1-x}\text{F}_x]\text{FeAs}$. *Chin Phys Lett*. 25:2215, and Qi YP, Gao ZS, Wang L, et al. (2008) Superconductivity in Co-doped SmFeAsO . *Supercond Sci Technol*, 21:115016.
3. Wang XC, Liu QQ, Lv YX, et al. (2008) The superconductivity at 18 K in LiFeAs system. *Solid State Commun*. 148:538-40 and Tapp JH, Tang ZJ, Lv B, et al. (2008) LiFeAs : An intrinsic FeAs -based superconductor with $T_c = 18$ K. *Phys Rev B*. 78:060505(R).
4. Guo J, Jin S, Wang G, et al. (2010) Superconductivity in the iron selenide $\text{K}_x\text{Fe}_2\text{Se}_2$ ($0 \leq x \leq 1.0$). *Phys Rev B* 82:180520(R). And Krzton-Maziopa A, Shermadini Z, Pomjakushina E, et al. (2011) Synthesis and crystal growth of $\text{Cs}_{0.8}(\text{FeSe}_{0.98})_2$: a new iron-based superconductor with $T_c = 27$ K. *J Phys: Condens Matter* 23:052203. And Fang MH, Wang HD, Dong CH, et al. (2011) Fe-based superconductivity with $T_c = 31$ K bordering an antiferromagnetic insulator in $(\text{Tl,K})\text{Fe}_x\text{Se}_2$. *EPL* 94:27009. And Ying JJ, Wang XF, Luo XG, et al. (2011) Superconductivity and magnetic properties of single crystals of $\text{K}_{0.75}\text{Fe}_{1.66}\text{Se}_2$ and $\text{Cs}_{0.81}\text{Fe}_{1.61}\text{Se}_2$. *Phys Rev B* 83:212502. And Wang AF, Ying JJ, Yan YJ, et al. (2011) Superconductivity at 32 K in single-crystalline $\text{RbFe}_{2-y}\text{Se}_2$. *Phys Rev B* 83:060512(R). And Li CH, Shen B, Han F, et al. (2011) Transport properties and anisotropy of $\text{Rb}_{1-x}\text{Fe}_{2-y}\text{Se}_2$ single crystals. *Phys Rev B* 83:184521.
5. Iyo A, Kawashima K, Kinjo T, et al. (2016) New-Structure-Type Fe-Based Superconductors: $\text{CaAFe}_4\text{As}_4$ ($A = \text{K, Rb, Cs}$) and $\text{SrAFe}_4\text{As}_4$ ($A = \text{Rb, Cs}$). *J Am Chem Soc* 138:3410-15.
6. Ogino H, Matsumura Y, Katsura Y, et al. (2009) Superconductivity at 17 K in $(\text{Fe}_2\text{P}_2)(\text{Sr}_4\text{Sc}_2\text{O}_6)$: a new superconducting layered pnictide oxide with a thick perovskite oxide layer. *Supercond Sci Technol* 22:075008. And Zhu X, Han F, Mu G, et al. (2009) Transition of stoichiometric $\text{Sr}_2\text{VO}_3\text{FeAs}$ to a superconducting state at 37.2 K. *Phys Rev B* 79:220512(R).
7. Ishida K, Nakai Y, Hosono H (2009) To What Extent Iron-Pnictide New Superconductors Have Been Clarified: A Progress Report. *J Phys Soc Jpn*, 78:062001.
8. Löhnert C, Stürzer T, Tegel M, et al. (2011) Superconductivity up to 35 K in the Iron Platinum Arsenides $(\text{CaFe}_{1-x}\text{Px}_x\text{As})_{10}\text{Pt}_{4-y}\text{As}_8$ with Layered Structures. *Angew Chem Int Ed* 50:9195-9.
9. Ni N, Allred JM, Chan BC, et al. (2011) High T_c electron doped $\text{Ca}_{10}(\text{Pt}_3\text{As}_8)(\text{Fe}_2\text{As}_2)_5$ and $\text{Ca}_{10}(\text{Pt}_4\text{As}_8)(\text{Fe}_2\text{As}_2)_5$ superconductors with skutterudite intermediary layers. *Proc Natl Acad Sci* 108:E1019-26.
10. Kakiya S, Kudo K, Nishikubo Y, et al. (2011) Superconducting Transition Temperatures of up to 47 K from Simultaneous Rare-Earth Element and Antimony Doping of 112-Type CaFeAs_2 . *J Phys Soc Jpn* 80:093704.
11. Kasinathan D, Ormeci A, Koch K, et al. (2009) AFe_2As_2 ($A = \text{Ca, Sr, Ba, Eu}$) and $\text{SrFe}_{2-x}\text{TM}_x\text{As}_2$ ($\text{TM} = \text{Mn, Co, Ni}$): crystal structure, charge doping, magnetism and superconductivity. *New J Phys* 11:025023.
12. Ren ZA, Zhao ZX (2009) Research and Prospects of Iron-Based Superconductors. *Adv Mater* 21:4584-92.
13. Rahmana A, Hossen A (2015) Brief Review on Iron-Based Superconductors Including Their Characteristics and Applications. *ASRJETS* 11:104-26.
14. Hosono H, Tanabe K, Takayama-Muromachi E, et al. (2015) Exploration of new superconductors and functional materials, and fabrication of superconducting tapes and wires of iron pnictides. *Sci Tech Adv Mater* 16:033503.

15. Ronning F, Klimczuk N, Bauer ED, et al. (2008) Synthesis and properties of CaFe_2As_2 single crystals. *J Phys: Condens Matter* 20:322201.
16. Krellner C, Caroca-Canales N, Jesche A, et al. (2008) Magnetic and structural transitions in layered iron arsenide systems: AFe_2As_2 versus RFeAsO . *Phys Rev B* 78:100504.
17. Rotter M, Tegel M, Schellenberg I, et al. (2008) Spin-density-wave anomaly at 140 K in the ternary iron arsenide BaFe_2As_2 . *Phys Rev B* 78:020503.
18. Jeevan HS, Hossain Z, Kasinathan D, et al. (2008) Antiferromagnetic transition in EuFe_2As_2 : A possible parent compound for superconductors. *Phys Rev B* 78:052501.
19. Jeevan HS, Hossain Z, Kasinathan D, et al. (2008) High-temperature superconductivity in $\text{Eu}_{0.5}\text{K}_{0.5}\text{Fe}_2\text{As}_2$. *Phys Rev B* 78:092406.
20. Leithe-Jasper A, Schnelle W, Geibel C, et al. (2008) Superconducting State in $\text{SrFe}_{2-x}\text{Co}_x\text{As}_2$ by Internal Doping of the Iron Arsenide Layers. *Phys Rev Lett* 101:207004.
21. Sefat AS, Jin R, McGuire VA, et al. (2008) Superconductivity at 22 K in Co-Doped BaFe_2As_2 Crystals. *Phys Rev Lett* 101:117004.
22. Kumar M, Nicklas M, Jesche A, et al. (2008) Effect of pressure on the magnetostructural transition in SrFe_2As_2 . *Phys Rev B* 78:184516.
23. Wu G, Chen H, Wu T, et al. (2008) Different resistivity response to spin-density wave and superconductivity at 20 K in $\text{Ca}_{1-x}\text{Na}_x\text{Fe}_2\text{As}_2$. *J Phys: Condens Matter* 20:422201 and Kumar N, Nagalakshmi R, Kulkarni R, et al. (2009) Anisotropic magnetic and superconducting properties of $\text{CaFe}_{2-x}\text{Co}_x\text{As}_2$ ($x = 0, 0.06$) single crystals. *Phys Rev B* 79:012504 and Ronning F, Klimczuk T, Bauer ED, et al. (2008) Synthesis and properties of CaFe_2As_2 single crystals. *J Phys: Condens Matter* 20:322201 and Shirage PV, Miyazawa K, Kito H, et al. (2008) Superconductivity at 26 K in $(\text{Ca}_{1-x}\text{Na}_x)\text{Fe}_2\text{As}_2$. *Appl Phys Express* 1:081702 and Ran S, Bud'ko SL, Straszheim WE, et al. (2012) Control of magnetic, nonmagnetic, and superconducting states in annealed $\text{Ca}(\text{Fe}_{1-x}\text{Co}_x)_2\text{As}_2$. *Phys Rev B* 85:224528 and Ran S, Bud'ko SL, Straszheim WE, et al. (2014) Combined effects of transition metal (Ni and Rh) substitution and annealing/quenching on the physical properties of CaFe_2As_2 . *Phys Rev B* 90:054501 and Gati E, Köhler S, Guterding D, et al. (2012) Hydrostatic-pressure tuning of magnetic, nonmagnetic, and superconducting states in annealed $\text{Ca}(\text{Fe}_{1-x}\text{Co}_x)_2\text{As}_2$. *Phys Rev B* 86:220511.
24. Uhoya W, Tsoi G, Vohra YK, et al. (2010) Anomalous compressibility effects and superconductivity of EuFe_2As_2 under high pressures. *J Phys: Condens Matter* 22:292202 and Bishop M, Uhoya W, Tsoi G, et al. (2010) Formation of collapsed tetragonal phase in EuCo_2As_2 under high pressure. *J Phys: Condens Matter* 22:425701.
25. Mittal R, Heid R, Bosak A, et al. (2010) Pressure dependence of phonon modes across the tetragonal to collapsed-tetragonal phase transition in CaFe_2As_2 . *Phys Rev B* 81:144502 and Kasahara S, Shibauchi T, Hashimoto K, et al. (2011) Abrupt recovery of Fermi-liquid transport following the collapse of the c axis in $\text{CaFe}_2(\text{As}_{1-x}\text{P}_x)_2$ single crystals. *Phys Rev B* 83:060505(R).
26. Danura M, Kudo K, Oshiro Y, et al. (2011) Interplay of Superconductivity and Fermi-Liquid Transport in Rh-Doped CaFe_2As_2 with Lattice-Collapse Transition. *J Phys Soc Jpn* 80:103701.
27. Gretarsson H, Saha SR, Drye T, et al. (2013) Spin-State Transition in the Fe Pnictides. *Phys Rev Lett* 110, 047003 and Ortenzi L, Gretarsson H, Kasahara S, et al. (2015) Structural Origin of the Anomalous Temperature Dependence of the Local Magnetic Moments in the CaFe_2As_2 Family of Materials. *Phys Rev Lett* 114:047001.
28. Nandi S, Kim MG, Kreyssig A, et al. (2010) Anomalous Suppression of the Orthorhombic Lattice Distortion in Superconducting $\text{Ba}(\text{Fe}_{1-x}\text{Co}_x)_2\text{As}_2$ Single Crystals. *Phys Rev Lett* 104:057006.
29. Avci S, Chmaissem O, Allred JM, et al. (2014) Magnetically driven suppression of nematic order in an iron-based supercon-

ductor. *Nat Commun* 5:3845.

30. Böhmer AE, Hardy F, Wang L, et al. (2015) Superconductivity-induced re-entrance of the orthorhombic distortion in $\text{Ba}_{1-x}\text{K}_x\text{Fe}_2\text{As}_2$. *Nat Commun* 6:7911.

31. Böhm T, Kretzschmar F, Baum A, et al. (2018) Microscopic origin of Cooper pairing in the iron-based superconductor $\text{Ba}_{1-x}\text{K}_x\text{Fe}_2\text{As}_2$. *npj Quantum Mater* 3:48 and Jost D, Peis L, He G, et al. (2022) Quantum critical fluctuations in an Fe-based superconductor. *Commun Phys* 5:201 and Lazarević N, Hackl R. (2020) Fluctuations and pairing in Fe-based superconductors: light scattering experiments. *J Phys: Condens Matter* 32:413001.

32. Ronning F, Klimczuk T, Bauer ED, et al. (2008) Synthesis and properties of CaFe_2As_2 single crystals. *J Phys: Condens Matter* 20:322201.

33. Ni N, Nandi S, Kreyssig A, et al. (2008) First-order structural phase transition in CaFe_2As_2 . *Phys Rev B* 78:014523 and Goldman AI, Argyriou DN, Ouladdiaf B, et al. (2008) Lattice and magnetic instabilities in CaFe_2As_2 : A single-crystal neutron diffraction study. *Phys Rev B* 78:100506 and Wu G, Chen H, Wu T, et al. (2008) Different resistivity response to spin-density wave and superconductivity at 20 K in $\text{Ca}_{1-x}\text{Na}_x\text{Fe}_2\text{As}_2$. *J Phys: Condens Matter* 20:422201 and Ronning F, Klimczuk T, Bauer ED, et al. (2008) Synthesis and properties of CaFe_2As_2 single crystals. *J Phys: Condens Matter* 20:322201 and Canfield PC, Bud'ko SL, Ni N, et al. (2009) Structural, magnetic and superconducting phase transitions in CaFe_2As_2 under ambient and applied pressure. *Physica C* 469:404–12 and Alzamora M, Munevar J, Baggio-Saitovitch E, et al. (2011) First-order phase transitions in CaFe_2As_2 single crystal: a local probe study. *J Phys: Condens Matter* 23:145701.

34. Choi KY, Wulferding D, Lemmens P, et al. (2008) Lattice and electronic anomalies of CaFe_2As_2 studied by Raman spectroscopy. *Phys Rev B* 78:212503.

35. Kumar P, Bera A, Muthu DVS, et al. (2011) Raman evidence for the superconducting gap and spin–phonon coupling in the superconductor $\text{Ca}(\text{Fe}_{0.95}\text{Co}_{0.05})_2\text{As}_2$. *J Phys: Condens Matter* 23: 255403.

36. Gale GD (1997) GULP: A computer program for the symmetry-adapted simulation of solids. *J Chem Soc, Faraday Trans* 93:629–37.

37. Litvinchuk AP, Hadjiev VG, Iliev MN, et al. (2008) Raman-scattering study of $\text{K}_x\text{Sr}_{1-x}\text{Fe}_2\text{As}_2$ ($x = 0.0, 0.4$). *Phys Rev B* 78:060503.

38. Kroumova E, Aroyo MI, Perez Mato JM, et al. (2003) Bilbao Crystallographic Server: Useful Databases and Tools for Phase-Transition Studies. *Phase Transitions* 76:155–70.

39. Saparov B, Cantoni C, Pan M. (2014) Complex structures of different CaFe_2As_2 samples. *Sci Rep* 4:4120. doi:10.1038/srep04120.

40. Gofryk K, Saparov B, Durakiewicz T, et al. (2014) Fermi-Surface Reconstruction and Complex Phase Equilibria in CaFe_2As_2 . *Phys Rev Lett* 112:186401.

41. Kreyssig A, Green MA, Lee Y, et al. (2008) Pressure-induced volume-collapsed tetragonal phase of CaFe_2As_2 as seen via neutron scattering. *Phys Rev B* 78:184517.

42. Goldman AI, Kreyssig A, Prokeš K, et al. (2009) Lattice collapse and quenching of magnetism in CaFe_2As_2 under pressure: A single-crystal neutron and x-ray diffraction investigation. *Phys Rev B* 79:024513.

43. Zhao K, Lv B, Deng L, et al. (2016) Interface-induced superconductivity at ~ 25 K at ambient pressure in undoped CaFe_2As_2 single crystals. *Proc Nat Acad Sci USA* 113:12968–73.

44. Ran S, Bud'ko SL, Pratt DK, et al. (2011) Stabilization of an ambient-pressure collapsed tetragonal phase in CaFe_2As_2 and tuning of the orthorhombic-antiferromagnetic transition temperature by over 70 K via control of nanoscale precipitates. *Phys*

Rev B 83:144517.

45. Ma C, Yang HX, Tian HF, et al. (2009) Microstructure and tetragonal-to-orthorhombic phase transition of AFe_2As_2 ($A = Sr, Ca$) as seen via transmission electron microscopy. *Phys Rev B* 79: 060506(R).
46. Huyan S, Deng LZ, Wu Z, et al. (2019) Low-temperature microstructural studies on superconducting $CaFe_2As_2$. *Sci Rep* 9:6393.
47. Ali K, Adhikary G, Thakur S, et al. (2018) Hidden phase in parent Fe-pnictide superconductors. *Phys Rev B* 97: 054505.
48. Pandeya RP, Pramanik A, Sakhya AP, et al. (2021) Evolution of local structure and superconductivity in $CaFe_2As_2$. *J Phys: Condens Matter* 33:19LT01.
49. Yildirim T. (2009) Strong Coupling of the Fe-Spin State and the As-As Hybridization in Iron-Pnictide Superconductors from First-Principle Calculations. *Phys Rev Lett* 102:037003.
50. Pashkevich YuG, Shevtsova TN, Gusev AA, et al. (2012) Spin state of iron—the control parameter of iron-containing HTSC: Dependence of ground state energy, phonon energies and atom positions on the spin state of iron ion in FeTe. *Low Temperature Physics* 38:900–3.
51. Balkanski M, Wallis RF, Haro E. (1983) Anharmonic effects in light scattering due to optical phonons in silicon. *Phys Rev B* 28:1928.
52. Glamazda A, Choi KY, Lemmens P, et al. (2015) Structural instability of the CoO_4 tetrahedral chain in $SrCoO_{3-\delta}$ thin films. *Appl Phys* 118:085313.
53. Khalyavin DD, Lovesey SW, Manuel P, et al. (2014) Symmetry of reentrant tetragonal phase in $Ba_{1-x}Na_xFe_2As_2$: Magnetic versus orbital ordering mechanism. *Phys Rev B* 90:174511.
54. Wang CP, Shieh SR, Withers AC, et al. (2020) Raman and X-ray diffraction study of pressure-induced phase transition in synthetic Mg_2TiO_4 . *Sci Rep* 10:6278.
55. Glamazda A, Choi YS, Do SH, et al. (2017) Quantum Criticality in the Coupled Two-Leg Spin Ladder Ba_2CuTeO_6 . *Phys Rev B* 95:184430.

Submit your next manuscript to Annex Publishers and benefit from:

- ▶ Easy online submission process
- ▶ Rapid peer review process
- ▶ Online article availability soon after acceptance for Publication
- ▶ Open access: articles available free online
- ▶ More accessibility of the articles to the readers/researchers within the field
- ▶ Better discount on subsequent article submission

Submit your manuscript at

<http://www.annexpublishers.com/paper-submission.php>